Journal of Integral Sciences
[An International Open Access Journal]
Available at www.jisciences.com ISSN: 2581-5679

ADSORPTIVE REMOVAL OF CONGO RED FROM AQUEOUS SOLUTION USING A CHITOSAN-*G*-POLY (ACRYLIC ACID-*CO*-ITACONIC ACID) HYDROGEL: EQUILIBRIUM, KINETICS AND THERMODYNAMICS

QUSAY K. MOJAR

Department of Chemistry, College of Education, University of Al-Qadisiyah, Diwaniya.

Received: 14-06-2026 Revised: 09-07-2026 Accepted: 23-08-2026

ABSTRACT

Textile effluent carrying Congo red (CR) is hard to treat, because the dye is highly soluble, chemically stable and toxic at low concentration. Here a hydrogel was prepared by graft copolymerising acrylic acid (AA) and itaconic acid (IA) onto chitosan, giving CH-*g*-poly(AA-*co*-IA), with potassium persulfate as initiator and N,N′-methylenebisacrylamide as crosslinker. It was examined by FTIR, XRD and FESEM, then tested on CR in batch mode. Uptake was strongly pH dependent: removal peaked at pH 3 (91.6 %) and fell to 14.2 % at pH 10, placing the protonated amine groups of the chitosan backbone at the centre of the binding step. A dose of 2 g L^{-1} removed more than 90 % of the dye from a 50 mg L^{-1} solution, and equilibrium was reached at about 210 min. Kinetic data were described best by the pseudo-second-order equation (R^2 = 0.9974 by non-linear fitting, 0.9991 in linear form); the intraparticle diffusion plot was multilinear, with a fast diffusion-controlled stage followed by a much slower approach to equilibrium. Equilibrium data followed the Freundlich model (R^2 = 0.9981, n = 2.20) more closely than the Langmuir model, which indicates an energetically heterogeneous surface; the Langmuir capacity was 100.7 mg g^{-1} at 298 K. The mean free energy from the Dubinin–Radushkevich model was 11.5 kJ mol^{-1}. Thermodynamic parameters ($\Delta H°$ = +22.92 kJ mol^{-1}, $\Delta S°$ = +88.74 J mol^{-1} K^{-1}, $\Delta G°$ = −2.61 to −6.14 kJ mol^{-1}) describe a spontaneous, endothermic and entropy-driven process.

Keywords: Congo red; chitosan; grafted hydrogel; itaconic acid; adsorption isotherm; thermodynamics.

This article is licensed under a Creative Commons Attribution-Non-commercial 4.0 International License.
Copyright © 2026 Author[s] retains the copyright of this article.

***Corresponding Author**
Qusay K. Mojar

DOI: https://doi.org/10.37022/jis.v9i2.155

Produced and Published by
South Asian Academic Publications

1. INTRODUCTION

Synthetic dyes are among the most conspicuous pollutants released by industry, and the textile sector loses a substantial fraction of what it applies; much of that load reaches surface water after only partial treatment [1,2]. Congo red is one of the more troubling members of the group. It is an anionic bis-azo dye built on a benzidine core, and reductive cleavage of its azo bonds can liberate mutagenic aromatic amines [1,3]. The molecule is also stubbornly stable: its two sulfonate groups keep it soluble over a wide pH range, while the extended conjugation resists light and mild oxidants [4,5]. Even at low concentration it colours water and limits light penetration in receiving streams [2].

Coagulation, membrane filtration, advanced oxidation and biological treatment have all been tried on dye-bearing effluent, and each carries a penalty cost, sludge, or incomplete mineralisation [6,7]. Adsorption has held its position because it is simple to operate, still works at low residual concentration, and allows the solid to be recovered [7,8]. Activated carbon remains the benchmark, but its price keeps pushing the search towards cheaper solids derived from biomass and biopolymers [9,10].

Chitosan is an obvious candidate: abundant, non-toxic and biodegradable, with amine groups that protonate in acidic media and, together with the hydroxyl groups, bind anionic dyes strongly [11,12]. The raw polymer swells and partly dissolves in dilute acid precisely the conditions under which anionic dyes are adsorbed best and both its surface area and its mechanical strength are low [13,14]. Grafting and crosslinking are the standard remedy, since attaching acidic vinyl monomers to the backbone introduces carboxyl functionality, stabilises the network and improves swelling [15,16].

This work reports a hydrogel in which acrylic acid and itaconic acid were graft copolymerised onto chitosan and crosslinked with N,N′-methylenebisacrylamide. Itaconic acid was chosen because it is bio-based and carries two carboxyl groups per repeat unit, raising the density of polar sites without an extra synthetic step [17, 18]. The material was characterised and then assessed for Congo red uptake against pH, dose, contact time, initial concentration and temperature.

2. MATERIALS AND METHODS

2.1. Chemicals

Chitosan (DD ≥ 75 %; medium molecular weight, 190–310 kDa), acrylic acid, itaconic acid, potassium persulfate (KPS) and N,N′-methylenebisacrylamide (MBA) were used as received from Sigma-Aldrich (analytical grade). Congo red ($C_{32}H_{22}N_6Na_2O_6S_2$, M_w = 696.66 g mol^{-1}, C.I. 22120) was supplied by Sigma-Aldrich (dye content ≥ 85 %). Hydrochloric acid and sodium hydroxide (Merck, analytical grade) were used for pH adjustment. All solutions were prepared in distilled water.

A stock solution of 1000 mg L^{-1} CR was prepared by dissolving the dye in distilled water, and working solutions were obtained by serial dilution. The maximum absorption wavelength was confirmed at 497 nm, and concentrations were read against a calibration curve (A = 0.0432C + 0.0051, R^2 = 0.9996; linear range 1–50 mg L^{-1}; LOD 0.18 mg L^{-1}).

2.2. Preparation of the CH-g-poly(AA-co-IA) hydrogel

The hydrogel was synthesised by free-radical graft copolymerisation, following the route used for related polysaccharide systems [16,19,20,21]. Chitosan (0.1–2.0 g) was dissolved in 30 mL of dilute acetic acid (2 % v/v) on a hot-plate stirrer at 50 °C for 30 min, with continuous stirring, until a homogeneous solution was obtained. Nitrogen was then bubbled through the solution to displace dissolved oxygen, and KPS (0.01–0.1 g, dissolved in 2 mL of water) was added under stirring to generate radicals on the backbone. Itaconic acid (0.3–1.5 g in 5 mL of water) was introduced next, followed by acrylic acid (1–10 mL). MBA (0.01–0.1 g in 5 mL of water) was added last as crosslinker, with stirring maintained and the nitrogen flow kept on throughout.

The mixture was transferred to glass tubes and held in a water bath at 70 °C for 2 h to complete polymerisation and network formation. The resulting gel was removed carefully, cut into discs of uniform size with a sharp blade, and washed with distilled water under stirring to displace unreacted monomer and soluble oligomer. The washing water was replaced every 30 min and monitored by UV-Vis spectrophotometry until the absorbance became constant. The discs were dried at 60 °C to constant weight, then ground and sieved repeatedly to give fine particles of uniform size. The optimised composition used in the adsorption work was chitosan 1.0 g : AA 5 mL : IA 0.5 g : KPS 0.05 g : MBA 0.05 g, with a grafting percentage of 285 % and a grafting efficiency of 82 %. The equilibrium swelling ratio in distilled water was 22.5 g g^{-1}. Figure 01 summarises the synthetic route and the interactions proposed between the network and the dye.

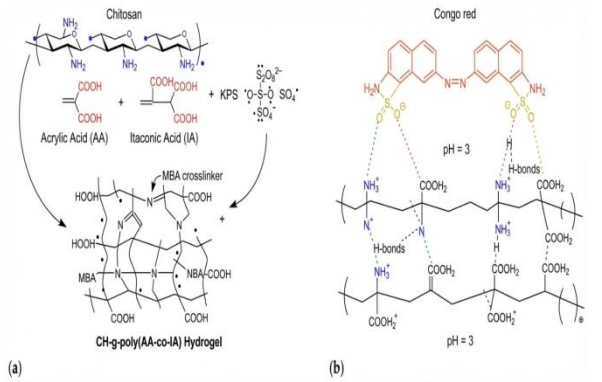

Figure 01: (a) Preparation of the CH-*g*-poly(AA-*co*-IA) hydrogel by free-radical graft copolymerisation of acrylic acid and itaconic acid onto chitosan, initiated by KPS and crosslinked with MBA; (b) interactions proposed between the protonated network and Congo red at pH 3.

2.3. Characterisation

Functional groups were identified by FTIR spectroscopy over 4000–400 cm^{-1} (Shimadzu FTIR-8400S, KBr disc). The crystalline character of chitosan and of the grafted network was compared by X-ray diffraction (Shimadzu XRD-6000, Cu Kα, λ = 1.5406 Å) over 2ϑ = 5–70° at a scan rate of 2° min^{-1}, with the tube operating at 40 kV and 30 mA. Surface morphology was imaged by field-emission scanning electron microscopy (TESCAN MIRA3 LMU, at an accelerating voltage of 15 kV) after gold coating. The point of zero charge was measured by the salt addition method in 0.01 mol L^{-1} NaCl, giving pH_{pzc} = 5.2.

2.4. Adsorption experiments

Batch experiments were carried out in 100 mL conical flasks holding 50 mL of dye solution, shaken at 180 rpm in a thermostatic shaker. Unless stated otherwise the runs used 50 mg L^{-1} CR, 0.1 g of adsorbent, pH 3 and 25 °C. The effect of pH was examined from 2 to 10 by adjusting with 0.1 mol L^{-1} HCl or NaOH; adsorbent dose was varied from 0.02 to 0.20 g per 50 mL (0.4–4.0 g L^{-1}); contact time was followed from 5 to 240 min; initial concentration was varied from 20 to 300 mg L^{-1}; and temperature was set at 15, 25, 35, 45 and 55 °C. After shaking, the suspensions were filtered and the residual dye was measured at 497 nm. All experiments were performed in triplicate and the results are reported as mean values; relative standard deviations were below 5 % in all cases.

The amount adsorbed at equilibrium, q_e (mg g^{-1}), and the removal efficiency, R (%), were obtained from Eqs (1) and (2):

$$q_e = (C_0 - C_e)V / m \quad (1)$$

$$R\ (\%) = [(C_0 - C_e) / C_0] \times 100 \quad (2)$$

where C_0 and C_e (mg L^{-1}) are the initial and equilibrium concentrations, V (L) is the solution volume and m (g) is the adsorbent mass. The amount adsorbed at time t was calculated in the same way, replacing C_e by C_t.

2.5. Modelling of the experimental data

Kinetic behaviour was tested against the pseudo-first-order (PFO) [22], pseudo-second-order (PSO) [23], intraparticle diffusion [24] and Elovich [25] equations, written here in their linear forms:

$$\ln(q_e - q_t) = \ln q_e - k_1 t \quad (3)$$

$$t/q_t = 1/(k_2 q_e^2) + t/q_e \quad (4)$$

$$q_t = k_{id} t^{1/2} + C \quad (5)$$

$$q_t = (1/\beta) \ln(\alpha\beta) + (1/\beta) \ln t \quad (6)$$

Equilibrium data were fitted to the Langmuir [26], Freundlich [27], Temkin [28] and Dubinin–Radushkevich (D–R) [29] isotherms:

$$C_e/q_e = 1/(K_L q_{max}) + C_e/q_{max} \quad (7)$$

$$R_L = 1/(1 + K_L C_0) \quad (8)$$

$$\log q_e = \log K_F + (1/n) \log C_e \quad (9)$$

$$q_e = B \ln A_T + B \ln C_e, \; B = RT/b_T \quad (10)$$

$$\ln q_e = \ln q_{DR} - \beta\varepsilon^2, \; \varepsilon = RT \ln(1 + 1/C_e), \; E = 1/(2\beta)^{1/2} \quad (11)$$

Because linear transformation redistributes the error and can favour one model artificially, the four isotherm equations and the pseudo-first-order, pseudo-second-order and Elovich equations were also fitted by non-linear least squares, and the two treatments are reported side by side [30,31]. The intraparticle diffusion equation was treated only in its linear form, since that is how its stages are read. Model quality was judged from the coefficient of determination, and RMSE and the average relative error (ARE) are given for the non-linear fits [32].

Thermodynamic parameters were obtained from the distribution constant $K_c = q_e/C_e$ using Eqs (12) and (13):

$$\Delta G^\circ = -RT \ln K_c \quad (12)$$

$$\ln K_c = \Delta S^\circ/R - \Delta H^\circ/(RT) \quad (13)$$

where R is the gas constant (8.314 J mol^{-1} K^{-1}) and T is the absolute temperature. The values of ΔH° and ΔS° were taken from the slope and intercept of ln K_c against $1/T$. It should be noted that K_c calculated as q_e/C_e carries units of L g^{-1}; the convention followed here is the one used most often in the adsorption literature, and the entropy term in particular shifts if the constant is first made dimensionless [33,34]. The comparison between temperatures, and the sign of ΔH°, are unaffected.

3. RESULTS AND DISCUSSION

3.1. Characterisation of the hydrogel

The FTIR spectra of chitosan and of CH-*g*-poly(AA-*co*-IA) are compared in Figure 02a. Chitosan shows the familiar broad envelope near 3430 cm^{-1} from overlapping O–H and N–H stretching, together with amide bands at about 1655 and 1595 cm^{-1}. After grafting, a strong carbonyl band appears at 1720 cm^{-1}, which is assigned to the carboxylic acid groups introduced by acrylic and itaconic acids, and the amide I region changes shape, consistent with reaction at the amine sites and with amide linkages from MBA. Bands near 1560 and 1405 cm^{-1} are attributed to the asymmetric and symmetric stretching of carboxylate, and the C–O–C skeletal band of the saccharide ring remains at about 1080 cm^{-1}, showing that the backbone survives the grafting step. Comparable band patterns have been reported for grafted chitosan hydrogels prepared with persulfate initiators [16, 35, 36].

X-ray diffraction (Figure 02b) shows the expected loss of order. Pristine chitosan gives reflections near 2ϑ = 10.5° and 20.1°, which correspond to its hydrated and crystalline forms; in the grafted product these merge into a single broad halo centred at 2ϑ = 21.8°. The same transition disappearance of the low-angle reflection and broadening of the main peak has been documented for graphene–chitosan and chitosan-*g*-poly(acrylic acid) hydrogels, and is taken as evidence that the grafted chains disrupt the hydrogen-bonded packing of the backbone [35,37]. An amorphous network of this type is advantageous for adsorption, since it swells more freely and exposes functional groups that would otherwise be locked inside a crystalline lattice.

FESEM images (Figure 02c and 02d) show the morphological change that accompanies the loss of crystallinity. Chitosan appears as smooth, dense and flake-like, with a relatively compact surface showing little porosity, whereas the hydrogel shows a rough, highly porous three-dimensional network with an irregular, sponge-like texture with pore openings in the range of 2–15 µm. A coarse, open surface of this kind provides both external area and channels through which the bulky dye can reach internal sites, and similar textures are reported for grafted polysaccharide hydrogels used as dye adsorbents [35,38].

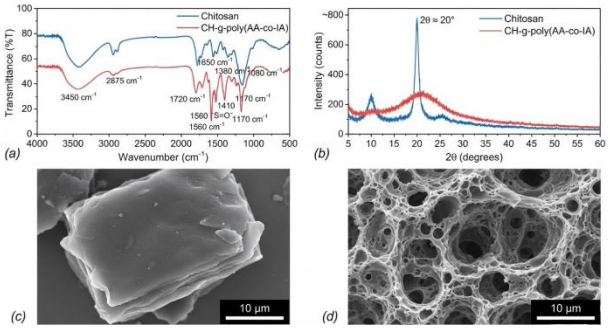

Figure 02: Characterisation of the prepared hydrogel: (a) FTIR spectra of chitosan and CH-*g*-poly(AA-*co*-IA); (b) XRD patterns of chitosan and CH-*g*-poly(AA-*co*-IA); (c) FESEM image of chitosan; (d) FESEM image of CH-*g*-poly(AA-*co*-IA).

3.2. Effect of solution pH

Solution pH governs both the charge on the adsorbent and the form of the dye, so it was examined first. Figure 03a shows removal rising from 87.2 % at pH 2 to a maximum of 91.6 % at pH 3, then falling steadily to

14.2 % at pH 10; the corresponding q_e values move from 21.80 to 22.90 and down to 3.55 mg g^{-1}.

The trend follows directly from the chemistry of the two partners. Congo red is a strong electrolyte whose sulfonate groups (pK_a below 1) stay dissociated as $–SO_3^-$ over the whole range studied. The hydrogel, in contrast, changes charge sharply. Below its point of zero charge the amine groups of the chitosan backbone are protonated to $–NH_3^+$ and the surface carries a net positive charge, so the dye anion is drawn in by electrostatic attraction [11,39]. The measured pH_{pzc} was 5.2; pH 3 lies well below this value, confirming that the surface carried a net positive charge under the optimum adsorption conditions. Above pH_{pzc} the amine groups lose their proton and the carboxylic acid groups of the grafted chains ionise to $–COO^-$. The surface then becomes negative, and repulsion between the two anions takes over; hydroxide ions compete for whatever positive sites remain [12,40]. The fall is steepest between pH 5 and pH 9, from 80.8 % to 24.8 %, which matches the deprotonation of the chitosan ammonium groups (pK_a near 6.3–6.5) rather than the ionisation of the grafted carboxyl groups; the latter are already largely dissociated by pH 6 and mainly add to the repulsion once the amine sites are lost.

The small decline at pH 2 deserves a comment. Two effects are likely to be at work. The chloride introduced with the acid used for adjustment may compete with the sulfonate groups for the protonated sites; and Congo red itself starts to protonate at its azo and amino nitrogens below about pH 3 the origin of its familiar red-to-blue colour change giving a form that is less soluble and aggregates more readily. Neither effect was isolated experimentally here, so this reading remains tentative. All later experiments were run at pH 3.

3.3. Effect of adsorbent dose

Increasing the dose from 0.4 to 4.0 g L^{-1} raised removal from 62.2 % to 93.8 %, while q_e fell from 77.75 to 11.73 mg g^{-1} (Figure 03b). The opposing trends have a common origin. More solid means more available sites, so a larger share of the dye is captured; but the sites added beyond a certain point go unused, because the dye left in solution has already been depleted, and dividing a nearly constant mass of adsorbed dye by a growing mass of solid drives q_e down. Particle aggregation at high loading, which shortens the effective diffusion path and buries part of the surface, contributes to the same effect [7].

The useful working point is where the curves flatten. Between 2.0 and 4.0 g L^{-1} removal improves by only 2.2 percentage points, so 2.0 g L^{-1} (0.1 g per 50 mL) was adopted for the remaining work as a reasonable compromise between efficiency and consumption of material.

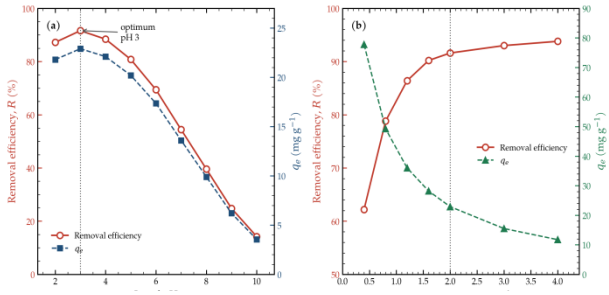

Figure 03: Effect of (a) solution pH and (b) adsorbent dose on the removal of Congo red by CH-*g*-poly(AA-*co*-IA). Conditions: C_0 = 50 mg L^{-1}, V = 50 mL, 180 rpm, 25 °C, 120 min; pH 3 in (b) and 0.1 g per 50 mL in (a).

3.4. Contact time and adsorption kinetics

The pH and dose series of Sections 3.2 and 3.3 were each run for a fixed 120 min; the kinetic series described here shows how close that is to equilibrium. A small between-batch variation was noted: the pH and dose series (each stopped at 120 min) gave 91.6 % removal under the same nominal conditions, whereas the kinetic run returned 87.8 % at 120 min. The difference is within the normal batch-to-batch scatter of hydrogel preparations, and the equilibrium values reported here are taken from the kinetic series, which was followed to completion. Uptake was rapid at first and then tailed off (Figure 04a). About 63 % of the final capacity was taken up within 30 min, 82 % within 60 min and 91 % within 90 min, after which the curve flattened; equilibrium was effectively reached at 210 min, with $q_{e,exp}$ = 22.90 mg g^{-1}. The early rise reflects the large number of vacant sites and the steep concentration gradient at the start. As those sites fill, the remaining dye has to travel further into the swollen network against increasing repulsion from molecules already bound, and the rate falls away.

Kinetic constants are collected in Table 01. The pseudo-second-order equation gave the closest description in both treatments, with R^2 = 0.9991 for the linear form and R^2 = 0.9974, ARE = 1.82 % for the non-linear fit, against 0.9852 and 0.9932 for the pseudo-first-order model. The pseudo-first-order line was fitted over 5–180 min, beyond which $q_e - q_t$ falls below the precision of the measurement and the logarithm becomes unstable. The pseudo-second-order rate constant was k_2 = 1.70 × 10^{-3} g mg^{-1} min^{-1}, giving an initial rate $h = k_2 q_e^2$ = 1.11 mg g^{-1} min^{-1}. One point should be made plainly: the pseudo-second-order model overestimates the equilibrium capacity ($q_{e,cal}$ = 25.54 mg g^{-1} against 22.90 mg g^{-1} measured), whereas the pseudo-first-order model returns 21.95 mg g^{-1}, much closer to experiment. The t/q_t plot is known to inflate R^2 because the transformation compresses the early points [31], so the two criteria are reported together rather than resolved in favour of one. Taken as a whole, the data support a rate step that depends on the interaction between dye and surface sites rather than on simple physical accumulation.

The intraparticle diffusion plot (Figure 04d) is not a single straight line, and it does not pass through the

origin. Two segments can be distinguished. The first, up to about 60 min, has $k_{id,1}$ = 2.665 mg g^{-1} $min^{-1/2}$ with an intercept close to zero (C = −0.95), which indicates that transport into the particle governs this stage with little boundary-layer resistance. The second segment is much shallower ($k_{id,2}$ = 0.503 mg g^{-1} $min^{-1/2}$) and has a large intercept (C = 15.80), the signature of a slow approach to equilibrium once the more accessible sites are occupied [24]. The size of the Congo red molecule, at 696.66 g mol^{-1}, is the most likely reason for the slowness of this second stage, although no smaller dye was run alongside it for comparison. The Elovich equation, with α = 2.52 mg g^{-1} min^{-1} and β = 0.193 g mg^{-1}, also gave a reasonable fit (R^2 = 0.9775) and points to an energetically non-uniform surface a conclusion that reappears in the equilibrium data.

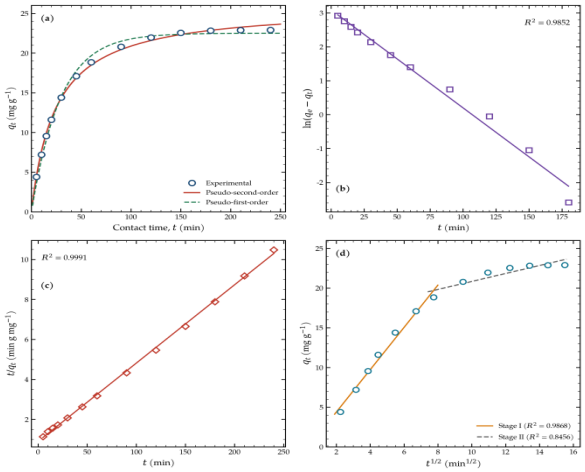

Figure 04: Adsorption kinetics of Congo red on CH-*g*-poly(AA-*co*-IA): (a) effect of contact time with non-linear pseudo-first-order and pseudo-second-order fits; (b) linear pseudo-first-order plot; (c) linear pseudo-second-order plot; (d) intraparticle diffusion plot showing two stages. Conditions: C_0 = 50 mg L^{-1}, 2 g L^{-1}, pH 3, 25 °C.

Table 01: Kinetic parameters for the adsorption of Congo red on CH-*g*-poly(AA-*co*-IA) (C_0 = 50 mg L^{-1}, 2 g L^{-1}, pH 3, 25 °C; $q_{e,exp}$ = 22.90 mg g^{-1}).

Model	Parameters	R^2	RMSE (mg g^{-1})	ARE (%)
Pseudo-first-order (linear, 5–180 min)	$q_{e,cal}$ = 21.95 mg g^{-1}; k_1 = 0.0289 min^{-1}	0.9852	–	–
Pseudo-first-order (non-linear)	$q_{e,cal}$ = 22.49 mg g^{-1}; k_1 = 0.0345 min^{-1}	0.9932	0.52	4.22
Pseudo-second-order (linear)	$q_{e,cal}$ = 25.54 mg g^{-1}; k_2 = 1.70 × 10^{-3} g mg^{-1} min^{-1}; h = 1.11 mg g^{-1} min^{-1}	0.9991	–	–
Pseudo-second-order (non-linear)	$q_{e,cal}$ = 25.94 mg g^{-1}; k_2 = 1.59 × 10^{-3} g mg^{-1} min^{-1}	0.9974	0.33	1.82
Intraparticle diffusion, stage I	$k_{id,1}$ = 2.665 mg g^{-1} $min^{-1/2}$; C = −0.95 mg g^{-1}	0.9868	–	–
Intraparticle diffusion, stage II	$k_{id,2}$ = 0.503 mg g^{-1} $min^{-1/2}$; C = 15.80 mg g^{-1}	0.8456	–	–
Elovich (linear)	α = 2.52 mg g^{-1} min^{-1}; β = 0.193 g mg^{-1}	0.9775	–	–
Elovich (non-linear)	α = 2.00 mg g^{-1} min^{-1}; β = 0.180 g mg^{-1}	0.9685	1.13	8.00

3.5. Adsorption isotherms

Equilibrium capacity rose from 9.20 to 86.60 mg g^{-1} as the initial concentration was raised from 20 to 300 mg L^{-1} (Figure 05a). The curve has no clear plateau over this range, which is the first indication that a strict monolayer description will not hold. Isotherm constants are given in Table 02.

Of the three surface-coverage models, the Freundlich equation described the data best. Linear regression gave K_F = 8.36 (mg g^{-1})(L mg^{-1})$^{1/n}$, $1/n$ = 0.494 and R^2 = 0.9911, and the non-linear fit gave K_F = 9.70, n = 2.20, R^2 = 0.9981 with ARE = 4.80 %. The Langmuir model was distinctly poorer (R^2 = 0.9771, ARE = 13.23 % non-linear), even though the linear plot of C_e/q_e against C_e looks acceptable at first sight. This is a useful reminder that a respectable linear R^2 can conceal a systematic misfit, which the error functions expose [30,32]. With n between 1 and 10 the process is classified as favourable, and a value of 2.20 suggests moderately strong binding on a surface whose sites differ in energy reasonable for a grafted network that carries amine, carboxyl and hydroxyl groups in an irregular arrangement.

The Langmuir parameters are still worth quoting for comparison, since most published capacities are expressed this way. They give q_{max} = 100.7 mg g^{-1} and K_L = 0.0332 L mg^{-1} at 298 K from the non-linear fit (97.6 mg g^{-1} and 0.0399 L mg^{-1} from the linear form). The separation factor R_L falls between 0.091 and 0.601 across the concentration range studied, confirming favourable adsorption throughout, and the decrease of R_L with rising C_0 is the expected pattern [32].

The Temkin model gave b_T = 139.9 J mol^{-1} and A_T = 0.639 L mg^{-1} with the weakest fit of the three (R^2 = 0.9513, ARE = 19.21 %). The small value of b_T points to a low average heat of adsorption and argues against a purely chemical interaction. The D–R model, on the other hand, returned a mean free energy E = 11.52 kJ mol^{-1} in its linear form and 11.63 kJ mol^{-1} by non-linear fitting, both inside the 8–16 kJ mol^{-1} window usually associated with chemisorption or ion exchange [41]. The two results are not contradictory so much as complementary: they suggest a mixed mechanism, with electrostatic ion-pair formation at the –NH_3^+ sites accompanied by weaker physical contributions elsewhere on a heterogeneous surface. The apparent D–R capacity (483 and 462 mg g^{-1} from the two treatments) is much larger than the Langmuir value, as is commonly observed, because the model refers to the total micropore volume rather than to a surface monolayer. It should be added that the D–R fit returns the highest R^2 of any equation tested (0.9995 non-linear). We have not used it to rank capacity, because it describes pore filling rather than surface coverage and its capacity term extrapolates far beyond the range actually measured; it is quoted here for the energy criterion alone.

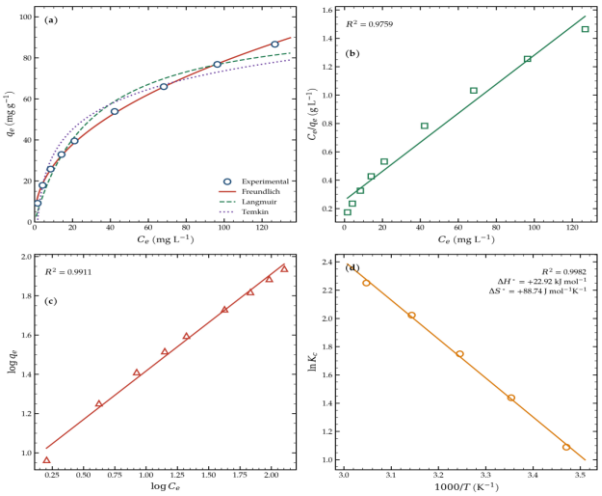

Figure 05: Equilibrium and thermodynamic behaviour: (a) adsorption isotherm with non-linear Langmuir, Freundlich and Temkin fits; (b) linear Langmuir plot; (c) linear Freundlich plot; (d) van 't Hoff plot. Conditions: 2 g L^{-1}, pH 3, 210 min; 25 °C in (a)–(c).

Table 02: Isotherm parameters for the adsorption of Congo red on CH-*g*-poly(AA-*co*-IA) (2 g L^{-1}, pH 3, 210 min, 25 °C).

Model	Parameters	R^2	RMSE (mg g^{-1})	ARE (%)
Langmuir (linear)	q_{max} = 97.65 mg g^{-1}; K_L = 0.0399 L mg^{-1}; R_L = 0.077–0.556	0.9759	–	–
Langmuir (non-linear)	q_{max} = 100.66 mg g^{-1}; K_L = 0.0332 L mg^{-1}; R_L = 0.091–0.601	0.9771	3.84	13.2
Freundlich (linear)	K_F = 8.36 (mg g^{-1})(L mg^{-1})$^{1/n}$; 1/n = 0.494; n = 2.02	0.9911	–	–
Freundlich (non-linear)	K_F = 9.70 (mg g^{-1})(L mg^{-1})$^{1/n}$; n = 2.20	0.9981	1.12	4.80
Temkin (linear and non-linear coincide)	A_T = 0.639 L mg^{-1}; b_T = 139.9 J mol^{-1}; $B = RT/b_T$ = 17.72 mg g^{-1}	0.9513	5.61	19.21
Dubinin–Radushkevich (linear)	q_{DR} = 483.0 mg g^{-1}; β = 3.77 × 10^{-9} mol^2 J^{-2}; E = 11.52 kJ mol^{-1}	0.9981	–	–
Dubinin–Radushkevich (non-linear)	q_{DR} = 462.1 mg g^{-1}; β = 3.69 × 10^{-9} mol^2 J^{-2}; E = 11.63 kJ mol^{-1}	0.9995	0.57	2.10

The Dubinin–Radushkevich model was evaluated with C_e in mol L^{-1} and q_e in mol g^{-1}.

3.6. Thermodynamic study

Raising the temperature from 288 to 328 K increased q_e from 21.40 to 23.75 mg g^{-1} and K_c from 2.97 to 9.50 L g^{-1}, so the process is endothermic. The van 't Hoff plot (Figure 05d) was linear over the whole interval (R^2 = 0.9982) and gave $\Delta H°$ = +22.92 kJ mol^{-1} and $\Delta S°$ = +88.74 J mol^{-1} K^{-1} (Table 03).

Values of $\Delta G°$ were negative at every temperature and grew more negative as the temperature rose, from −2.61 kJ mol^{-1} at 288 K to −6.14 kJ mol^{-1} at 328 K, so adsorption is spontaneous and is favoured by heating. The magnitude of $\Delta G°$ is often used to separate physical from chemical adsorption, but that reading has to be treated cautiously here. With K_c expressed in L g^{-1} the values fall below 20 kJ mol^{-1}, which would suggest physisorption; if K_c is first rendered dimensionless by the usual factor of 10^3, $\Delta G°$ at 298 K becomes −20.7 kJ mol^{-1} and $\Delta S°$ rises to 146.2 J mol^{-1} K^{-1}, while $\Delta H°$ is unchanged [33,34]. The classification therefore depends on a convention rather than on the data, and we do not rest any mechanistic claim on it. The sign of $\Delta H°$ is robust, and a positive value is consistent with a step that requires desolvation: both the dye anion and the protonated amine sites carry

hydration shells, and stripping them costs more energy than the ion pair subsequently releases.

The same desolvation accounts for the positive entropy. Releasing ordered water molecules from two charged partners into the bulk raises the disorder of the system, and under either convention $T\Delta S°$ exceeds $\Delta H°$ across the range studied, so it is the entropy term that carries $\Delta G°$ below zero.

Table 03: Thermodynamic parameters for the adsorption of Congo red on CH-*g*-poly(AA-*co*-IA) (C_0 = 50 mg L^{-1}, 2 g L^{-1}, pH 3, 210 min).

T (K)	q_e (mg g^{-1})	K_c (L g^{-1})	ln K_c	$\Delta G°$ (kJ mol^{-1})	$\Delta H°$ (kJ mol^{-1})	$\Delta S°$ (J mol^{-1} K^{-1})
288.15	21.40	2.97	1.089	−2.61		
298.15	22.35	4.22	1.439	−3.57		
308.15	23.00	5.75	1.749	−4.48	+22.92	+88.74
318.15	23.45	7.56	2.023	−5.35		
328.15	23.75	9.50	2.251	−6.14		

Values of $\Delta H°$ and $\Delta S°$ were obtained from the van 't Hoff plot (R^2 = 0.9982).

3.7. Proposed adsorption mechanism

Taken together, the results support the picture drawn in Figure 01b. The dominant interaction is electrostatic. At pH 3 the backbone amine groups exist as $–NH_3^+$, and each Congo red molecule offers two $–SO_3^-$ groups, so a single dye molecule can bridge two adjacent sites. Bidentate anchoring of this kind would strengthen the attachment relative to a single ion pair, although no mono-sulfonated dye was examined here, so the point remains a structural inference rather than a measured comparison. What the data do establish is the sharp pH dependence of Section 3.2, which is difficult to explain without an electrostatic step.

Electrostatics alone, however, does not account for everything. Hydrogen bonding is available between the hydroxyl and un-ionised carboxyl groups of the network and the amino, azo and sulfonate groups of the dye; at pH 3 most carboxyl groups are protonated and therefore act as donors rather than as competing anions, which is part of why the acidic optimum is so pronounced. The aromatic naphthalene and biphenyl rings of Congo red can also enter n–π interactions with the carbonyl and amide groups of the grafted chains; the network itself carries no aromatic rings, so any π–π stacking would have to occur between dye molecules already bound, which becomes plausible only at higher loading. Neither interaction was probed directly here. Finally, the swollen network offers channels for the dye to diffuse into, and the multilinear diffusion plot shows that this pathway contributes measurably to the overall rate.

The heterogeneity implied by the Freundlich exponent and by the Elovich fit falls neatly into this scheme. Sites of at least three kinds are present protonated amine, carboxyl and hydroxyl and they differ both in binding energy and in accessibility, some at the outer surface, others deep within the network.

3.8. Comparison with reported adsorbents

Table 04 sets the present capacity against values reported for other chitosan-based and polymeric adsorbents of Congo red. The comparison should be read with care, because reported capacities depend heavily on the concentration range covered, the dose, the pH and the way the isotherm was fitted; a Langmuir q_{max} extracted from data that never approach saturation is an extrapolation, not a measurement.

With that caveat, 100.7 mg g^{-1} places CH-*g*-poly(AA-*co*-IA) in the middle of the published field. It is very close to the bis-uracil crosslinked chitosan hydrogel (93.5 mg g^{-1}) [42] and to the itaconic acid-modified layered double hydroxide/gellan gum nanocomposite (99.9 mg g^{-1}) [43], and well above simple mineral and agricultural adsorbents such as fly ash (22.1 mg g^{-1}) [44] and untreated sorghum husk (57.6 mg g^{-1}; 77.1 mg g^{-1} after acid treatment) [45]. It is an order of magnitude below the best performers, notably the chitosan/poly(DDA-co-acrylamide) semi-interpenetrating hydrogel (1803.5 mg g^{-1}) [46] and the dialdehyde-cellulose-crosslinked cellulose–chitosan foam (1548.2 mg g^{-1}) [47], both of which were evaluated at far higher initial concentrations. It also improves substantially on the MWCNT/chitosan-g-poly(acrylic acid–crotonic acid) composite (14.1 mg g^{-1}) [48], which is the closest structural analogue of the present material. The two studies differ in more than the second monomer, so the gap cannot be assigned to itaconic acid alone; a side-by-side preparation of the two copolymers under identical conditions would settle the point and seems worth doing.

Table 04: Maximum adsorption capacities reported for Congo red on chitosan-based and related polymeric adsorbents.

Adsorbent	q_{max} (mg g^{-1})	Optimum pH	Best isotherm	Ref.
MWCNT/chitosan-g-poly(AA-co-crotonic acid)	14.13	n.r.	Langmuir	[48]
Fly ash (unmodified industrial waste)	22.12	natural	Langmuir	[44]
Chitosan-diatomite/calcium alginate beads	48.42	7	Langmuir	[49]
Activated carbon (Spathodea campanulata)	59.27	7	Langmuir	[9]

Adsorbent	q_{max} (mg g^{-1})	Optimum pH	Best isotherm	Ref.
Sorghum husk (acid-treated)	77.14	2	Langmuir	[45]
Bis-uracil crosslinked chitosan hydrogel	93.46	4	Langmuir	[42]
Itaconic acid-modified LDH/gellan gum	99.90	5	Freundlich	[43]
CH-*g*-poly(AA-*co*-IA) hydrogel (this work)	100.70	3	Freundlich	This work
Lignin/chitosan beads	173.00	3	n.r.	[50]
Chitosan-glutaraldehyde-β-cyclodextrin/ZnO	337.00	acidic	Liu / Langmuir	[51]
Coffee-grounds cellulose/sodium alginate beads	411.45	n.r.	Langmuir-Freundlich	[52]
CTAB-modified orange peel biochar	609.80	3	Langmuir	[10]
Polypyrrole/algal dead biomass composite	772.70	5	Freundlich	[53]
Dialdehyde-cellulose-crosslinked cellulose-chitosan foam	1548.20	n.r.	Sips	[47]
Chitosan/poly(DDA-co-acrylamide) hydrogel	1803.51	4-10	Hill	[46]
Lignosulfonate/hyperbranched polyamide amine hydrogel	5120.00	natural	Langmuir	[54]

n.r. = not reported. Capacities were determined under different experimental conditions and are therefore indicative rather than strictly comparable.

Two limitations of the present study should be stated. Regeneration and reuse were not examined, and they matter for any practical assessment; the carboxyl-rich network should in principle desorb Congo red in alkaline medium, but this needs to be demonstrated over several cycles. Performance in real textile effluent, where competing anions, surfactants and salinity are present, also remains to be tested. [Add regeneration and real-effluent results here if data are available.]

4. CONCLUSION

Acrylic acid and itaconic acid were grafted onto chitosan and crosslinked with MBA, and the resulting hydrogel removed Congo red efficiently from water. Removal was strongly pH dependent, reaching 91.6 % at pH 3 and collapsing in alkaline medium, which identifies the protonated backbone amine groups as the principal binding sites for the sulfonate groups of the dye. A dose of 2 g L^{-1} and 210 min of contact were sufficient. Kinetics followed the pseudo-second-order equation, and the multilinear intraparticle diffusion plot separated a fast diffusion-controlled stage from a much slower approach to equilibrium. Equilibrium data fitted Freundlich better than Langmuir, indicating an energetically heterogeneous surface; the Langmuir capacity was 100.7 mg g^{-1} at 298 K, and the Dubinin–Radushkevich energy of 11.5 kJ mol^{-1} lay in the range usually linked with chemisorption or ion exchange. Adsorption was spontaneous and endothermic, the positive entropy change pointing to desolvation as the driving step. The material is simple to prepare from inexpensive reagents, and its capacity matches several modified chitosan hydrogels, although it stays an order of magnitude below the best performers reported so far. Regeneration and trials with real effluent are the obvious next steps.

5. AUTHOR CONTRIBUTIONS

[Author 1]: Conceptualisation, Methodology, Investigation, Formal analysis, Writing – original draft. [Author 2]: Conceptualisation, Supervision, Writing – review and editing.

6. CONFLICTS OF INTEREST

The authors declare no conflict of interest.

7. DATA AVAILABILITY

The data supporting the findings of this study are available from the corresponding author on reasonable request.

8. ACKNOWLEDGEMENTS

The authors thank the Department of Chemistry, College of Education, University of Al-Qadisiyah for providing the laboratory facilities. [Add any funding information, or state: No external funding was received for this study.]

9. REFERENCES

1. Oladoye, P.O.; Bamigboye, M.O.; Ogunbiyi, O.D.; Akano, M.T. Toxicity and decontamination strategies of Congo red dye. Groundwater for Sustainable Development 2022, 19, 100844. https://doi.org/10.1016/j.gsd.2022.100844
2. Berradi, M.; Hsissou, R.; Khudhair, M.; Assouag, M.; Cherkaoui, O.; El Bachiri, A.; et al. Textile finishing dyes and their impact on aquatic environs. Heliyon 2019, 5 (11), e02711. https://doi.org/10.1016/j.heliyon.2019.e02711

3. Siddiqui, S.I.; Allehyani, E.S.; Al-Harbi, S.A.; Hasan, Z.; Abomuti, M.A.; Rajor, H.K.; et al. Investigation of Congo red toxicity towards different living organisms: a review. Processes 2023, 11 (3), 807. https://doi.org/10.3390/pr11030807
4. Al-Tohamy, R.; Ali, S.S.; Li, F.; Okasha, K.M.; Mahmoud, Y.A.-G.; Elsamahy, T.; et al. A critical review on the treatment of dye-containing wastewater: ecotoxicological and health concerns of textile dyes and possible remediation approaches for environmental safety. Ecotoxicology and Environmental Safety 2022, 231, 113160. https://doi.org/10.1016/j.ecoenv.2021.113160
5. Ben Slama, H.; Chenari Bouket, A.; Pourhassan, Z.; Alenezi, F.N.; Silini, A.; Cherif-Silini, H.; et al. Diversity of synthetic dyes from textile industries, discharge impacts and treatment methods. Applied Sciences 2021, 11 (14), 6255. https://doi.org/10.3390/app11146255
6. Rashid, R.; Shafiq, I.; Akhter, P.; Iqbal, M.J.; Hussain, M. A state-of-the-art review on wastewater treatment techniques: the effectiveness of adsorption method. Environmental Science and Pollution Research 2021, 28 (8), 9050-9066. https://doi.org/10.1007/s11356-021-12395-x
7. Dutta, S.; Gupta, B.; Srivastava, S.K.; Gupta, A.K. Recent advances on the removal of dyes from wastewater using various adsorbents: a critical review. Materials Advances 2021, 2 (14), 4497-4531. https://doi.org/10.1039/D1MA00354B
8. Strebel, A.; Behringer, M.; Hilbig, H.; Machner, A.; Helmreich, B. Anionic azo dyes and their removal from textile wastewater through adsorption by various adsorbents: a critical review. Frontiers in Environmental Engineering 2024, 3, 1347981. https://doi.org/10.3389/fenve.2024.1347981
9. Sudarsan, S.; Murugesan, G.; Varadavenkatesan, T.; Vinayagam, R.; Selvaraj, R. Efficient adsorptive removal of Congo red dye using activated carbon derived from Spathodea campanulata flowers. Scientific Reports 2025, 15, 1831. https://doi.org/10.1038/s41598-025-86032-9
10. Hua, Z.; Pan, Y.; Hong, Q. Adsorption of Congo red dye in water by orange peel biochar modified with CTAB. RSC Advances 2023, 13 (18), 12502-12508. https://doi.org/10.1039/D3RA01444D
11. Aramesh, N.; Bagheri, A.R.; Bilal, M. Chitosan-based hybrid materials for adsorptive removal of dyes and underlying interaction mechanisms. International Journal of Biological Macromolecules 2021, 183, 399-422. https://doi.org/10.1016/j.ijbiomac.2021.04.158
12. Pal, P.; Pal, A.; Nakashima, K.; Yadav, B.K. Applications of chitosan in environmental remediation: a review. Chemosphere 2021, 266, 128934. https://doi.org/10.1016/j.chemosphere.2020.128934
13. Agha, H.M.; Jawad, A.H. A review on the influence of crosslinking and grafting processes on the adsorptive performance of chitosan biopolymer for dyes removal. Next Bioengineering 2025, 1, 100007. https://doi.org/10.1016/j.nxbio.2025.100007
14. Yin, S.; Yuan, W.; Zhao, L.; Niu, Y.; Guo, J. Chitosan hydrogels for antibiotic remediation and dye removal: a review. Gels 2026, 12 (8), 658. https://doi.org/10.3390/gels12080658
15. Patel, R.; Trivedi, R.; Raj, M.; Raj, L. Graft copolymerization of chitosan with various monomers: a comprehensive review. Polymer Bulletin 2025, 82 (17), 11551-11591. https://doi.org/10.1007/s00289-025-06002-z
16. Phonlakan, K.; Meetam, P.; Chonlaphak, R.; Kongseng, P.; Chantarak, S.; Budsombat, S. Poly(acrylic acid-co-2-acrylamido-2-methyl-1-propanesulfonic acid)-grafted chitosan hydrogels for effective adsorption and photocatalytic degradation of dyes. RSC Advances 2023, 13 (44), 31002-31016. https://doi.org/10.1039/D3RA05596E
17. Choi, H.; Park, J.; Lee, J. Sustainable bio-based superabsorbent polymer: poly(itaconic acid) with superior swelling properties. ACS Applied Polymer Materials 2022, 4 (6), 4098-4108. https://doi.org/10.1021/acsapm.2c00021
18. Sangeetha, E.; Narayanan, A.; Dhamodharan, R. Super water-absorbing hydrogel based on chitosan, itaconic acid and urea: preparation, characterization and reversible water absorption. Polymer Bulletin 2022, 79 (5), 3013-3030. https://doi.org/10.1007/s00289-021-03641-w
19. Mohammadzadeh Pakdel, P.; Peighambardoust, S.J.; Arsalani, N.; Aghdasinia, H. Safranin-O cationic dye removal from wastewater using carboxymethyl cellulose-grafted-poly(acrylic acid-co-itaconic acid) nanocomposite hydrogel. Environmental Research 2022, 212, 113201. https://doi.org/10.1016/j.envres.2022.113201
20. Sayyar, Z.; Mohammadzadeh Pakdel, P.; Peighambardoust, S.J. Oral delivery of Sunitinib malate using carboxymethyl cellulose/poly(acrylic acid-itaconic acid)/Cloisite 30B nanocomposite hydrogel as a pH-responsive carrier. BMC Biotechnology 2024, 24 (1), 70. https://doi.org/10.1186/s12896-024-00883-0
21. Penyan, W.L.; Jasim, L.S. Preparation and characterization of a novel pH-sensitive pectin-grafted-poly(acrylic acid-co-itaconic acid)/MWCNTs-COOH hydrogel composite for adsorption and controlled release of diclofenac sodium. Carbon Letters 2024, 34 (5), 1413-1429. https://doi.org/10.1007/s42823-024-00702-8
22. Lagergren, S. Zur Theorie der sogenannten Adsorption gelöster Stoffe. Kungliga Svenska Vetenskapsakademiens Handlingar 1898, 24 (4), 1-39.

23. Ho, Y.S.; McKay, G. Pseudo-second order model for sorption processes. Process Biochemistry 1999, 34 (5), 451-465. https://doi.org/10.1016/S0032-9592(98)00112-5
24. Weber, W.J., Jr.; Morris, J.C. Kinetics of adsorption on carbon from solution. Journal of the Sanitary Engineering Division (ASCE) 1963, 89 (2), 31-59. https://doi.org/10.1061/JSEDAI.0000430
25. Chien, S.H.; Clayton, W.R. Application of Elovich equation to the kinetics of phosphate release and sorption in soils. Soil Science Society of America Journal 1980, 44 (2), 265-268. https://doi.org/10.2136/sssaj1980.03615995004400020013x
26. Langmuir, I. The adsorption of gases on plane surfaces of glass, mica and platinum. Journal of the American Chemical Society 1918, 40 (9), 1361-1403. https://doi.org/10.1021/ja02242a004
27. Freundlich, H. Über die Adsorption in Lösungen. Zeitschrift für Physikalische Chemie 1906, 57U (1), 385-470. https://doi.org/10.1515/zpch-1907-5723
28. Temkin, M.I.; Pyzhev, V. Kinetics of ammonia synthesis on promoted iron catalysts. Acta Physicochimica URSS 1940, 12, 217-222.
29. Dubinin, M.M.; Radushkevich, L.V. Equation of the characteristic curve of activated charcoal. Proceedings of the Academy of Sciences of the USSR, Physical Chemistry Section 1947, 55, 331-333.
30. Wang, J.; Guo, X. Adsorption isotherm models: classification, physical meaning, application and solving method. Chemosphere 2020, 258, 127279. https://doi.org/10.1016/j.chemosphere.2020.127279
31. Wang, J.; Guo, X. Adsorption kinetic models: physical meanings, applications, and solving methods. Journal of Hazardous Materials 2020, 390, 122156. https://doi.org/10.1016/j.jhazmat.2020.122156
32. Al-Ghouti, M.A.; Da'ana, D.A. Guidelines for the use and interpretation of adsorption isotherm models: a review. Journal of Hazardous Materials 2020, 393, 122383. https://doi.org/10.1016/j.jhazmat.2020.122383
33. Lima, E.C.; Hosseini-Bandegharaei, A.; Moreno-Piraján, J.C.; Anastopoulos, I. A critical review of the estimation of the thermodynamic parameters on adsorption equilibria. Wrong use of equilibrium constant in the Van't Hoof equation for calculation of thermodynamic parameters of adsorption. Journal of Molecular Liquids 2019, 273, 425-434. https://doi.org/10.1016/j.molliq.2018.10.048
34. Tran, H.N. Improper estimation of thermodynamic parameters in adsorption studies with distribution coefficient KD (qe/Ce) or Freundlich constant (KF): considerations from the derivation of dimensionless thermodynamic equilibrium constant and suggestions. Adsorption Science & Technology 2022, 2022, 5553212. https://doi.org/10.1155/2022/5553212
35. Thamer, B.M.; Aldalbahi, A.; Moydeen A., M.; El-Newehy, M.H. In situ preparation of novel porous nanocomposite hydrogel as effective adsorbent for the removal of cationic dyes from polluted water. Polymers 2020, 12 (12), 3002. https://doi.org/10.3390/polym12123002
36. Farasati Far, B.; Naimi-Jamal, M.R.; Jahanbakhshi, M.; Keihankhadiv, S.; Baradarbarjastehbaf, F. Enhanced methylene blue adsorption using single-walled carbon nanotubes/chitosan-graft-gelatin nanocomposite hydrogels. Scientific Reports 2024, 14, 19217. https://doi.org/10.1038/s41598-024-69969-1
37. Omidi, S.; Kakanejadifard, A. Eco-friendly synthesis of graphene-chitosan composite hydrogel as efficient adsorbent for Congo red. RSC Advances 2018, 8 (22), 12179-12189. https://doi.org/10.1039/C8RA00510A
38. Ferfera-Harrar, H.; Benhalima, T.; Sadi, A. Development of functional chitosan-based superabsorbent hydrogel nanocomposites for adsorptive removal of Basic Red 46 textile dye. Polymer Bulletin 2022, 79 (8), 6141-6172. https://doi.org/10.1007/s00289-021-03795-7
39. Abdelaziz, R.M.; El-Maghraby, A.; Sadik, W.A.; El-Demerdash, A.-G.M.; Fadl, E.A. Biodegradable cellulose nanocrystals hydrogels for removal of acid red 8 dye from aqueous solutions. Scientific Reports 2022, 12, 6424. https://doi.org/10.1038/s41598-022-10087-1
40. Poornachandhra, C.; Jayabalakrishnan, R.M.; Prasanthrajan, M.; Balasubramanian, G.; Lakshmanan, A.; Selvakumar, S.; et al. Cellulose-based hydrogel for adsorptive removal of cationic dyes from aqueous solution: isotherms and kinetics. RSC Advances 2023, 13 (7), 4757-4774. https://doi.org/10.1039/D2RA08283G
41. Hu, Q.; Zhang, Z. Application of Dubinin-Radushkevich isotherm model at the solid/solution interface: a theoretical analysis. Journal of Molecular Liquids 2019, 277, 646-648. https://doi.org/10.1016/j.molliq.2019.01.005
42. Alharbi, R.A.; Alminderej, F.M.; Al-Harby, N.F.; Elmehbad, N.Y.; Mohamed, N.A. Preparation and characterization of a new bis-uracil chitosan-based hydrogel as efficient adsorbent for removal of anionic Congo red dye. Polymers 2023, 15 (6), 1529. https://doi.org/10.3390/polym15061529
43. Shabani, S.; Dinari, M. Itaconic acid-modified layered double hydroxide/gellan gum nanocomposites for Congo red adsorption. Scientific Reports 2022, 12 (1), 4356. https://doi.org/10.1038/s41598-022-08414-7
44. Harja, M.; Buema, G.; Bucur, D. Recent advances in removal of Congo red dye by adsorption using an industrial waste. Scientific Reports 2022, 12, 6087. https://doi.org/10.1038/s41598-022-10093-3
45. Din, S.U.; Ofudje, E.A.; Al-Ahmary, K.M.; Alqahtani, Z.; Al-Mhyawi, S.R.; Alshdoukhi, I.F.; et al. Sorghum husks as potential low cost adsorbent for Congo

red adsorption. Scientific Reports 2025, 15, 38265. https://doi.org/10.1038/s41598-025-22082-3

46. Liu, H.; Zhang, H.; Ye, Z.; Xiong, G. Efficient removal of anionic dye Congo red by chitosan/poly(dimethyl diallyl ammonium chloride-co-acrylamide) composite hydrogel. International Journal of Biological Macromolecules 2025, 294, 139462. https://doi.org/10.1016/j.ijbiomac.2025.139462
47. Kim, U.-J.; Kimura, S.; Wada, M. Highly enhanced adsorption of Congo red onto dialdehyde cellulose-crosslinked cellulose-chitosan foam. Carbohydrate Polymers 2019, 214, 294-302. https://doi.org/10.1016/j.carbpol.2019.03.058
48. Mahdi, K.M.; Almansarawi, S.A.; Jasim, L.S.; Batool, M. Efficient adsorption of Congo red dye from aqueous solution using MWCNT/chitosan-*g*-poly(acrylic acid-crotonic acid) composite. Applied Chemical Engineering 2025, 8 (3), 5729. https://doi.org/10.59429/ace.v8i3.5729
49. Zhao, D.; Shen, X. Preparation of chitosan-diatomite/calcium alginate composite hydrogel beads for the adsorption of Congo red dye. Water 2023, 15 (12), 2254. https://doi.org/10.3390/w15122254
50. Han, X.; Li, R.; Miao, P.; Gao, J.; Hu, G.; Zhao, Y.; et al. Design, synthesis and adsorption evaluation of bio-based lignin/chitosan beads for Congo red removal. Materials 2022, 15 (6), 2310. https://doi.org/10.3390/ma15062310
51. Sirach, R.; Dave, P.N. Glutaraldehyde crosslinked chitosan-β-cyclodextrin/ZnO composite for the effective adsorption of Congo red anionic dye. Carbohydrate Polymer Technologies and Applications 2025, 10, 100835. https://doi.org/10.1016/j.carpta.2025.100835
52. Kasbaji, M.; Mennani, M.; Grimi, N.; Oubenali, M.; Mbarki, M.; El Zakhem, H.; et al. Adsorption of cationic and anionic dyes onto coffee grounds cellulose/sodium alginate double-network hydrogel beads: isotherm analysis and recyclability performance. International Journal of Biological Macromolecules 2023, 239, 124288. https://doi.org/10.1016/j.ijbiomac.2023.124288
53. Maqbool, M.; Sadaf, S.; Bhatti, H.N.; Rehmat, S.; Kausar, A.; Alissa, S.A.; et al. Sodium alginate and polypyrrole composites with algal dead biomass for the adsorption of Congo red dye: kinetics, thermodynamics and desorption studies. Surfaces and Interfaces 2021, 25, 101183. https://doi.org/10.1016/j.surfin.2021.101183
54. Li, R.; Tian, N.; Jiang, J.; Wu, D.; Xia, M.; Ni, H.; et al. Lignosulfonate-based hybrid hydrogels functionalized with hyperbranched polyamide amine as ultra-high-capacity adsorbent for Congo red removal from aqueous solutions. Water, Air, & Soil Pollution 2023, 234 (3), 140. https://doi.org/10.1007/s11270-023-06162-6